SUPPLEMENTARY INFORMATION

Intrinsic Chemistry of $[OUCH]^+$: Reactions with H_2O, $CH_3C{\equiv}N$ and O_2

Luke J. Metzler[1], Christopher T. Farmen[1], Theodore A. Corcovilos[2]
and Michael J. Van Stipdonk[1*]
[1]Department of Chemistry and Biochemistry, Duquesne University, USA
[2]Department of Physics, Duquesne University, USA

SUPPLEMENTARY INFORMATION

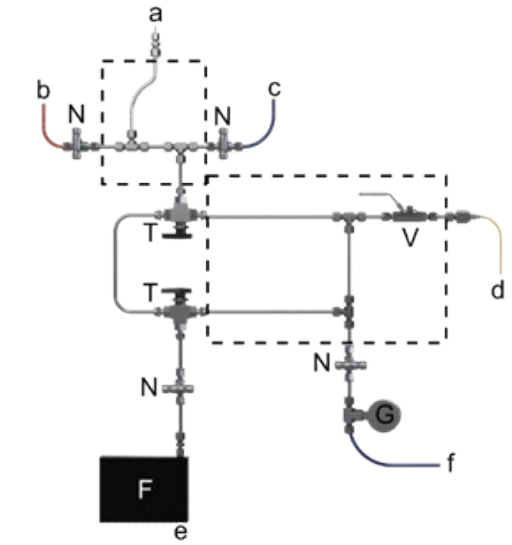

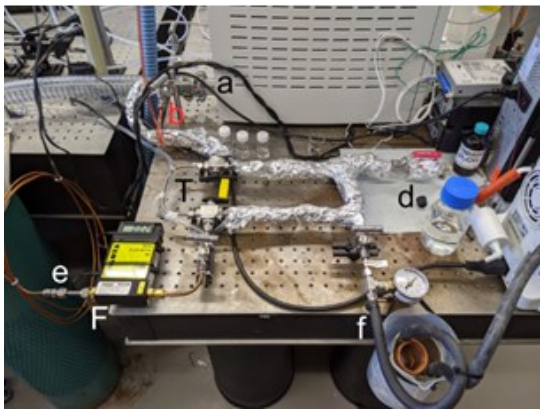

Figure S1. The gas manifold on the buffer gas inlet of the ion trap instrument (labels below refer to this figure) to allow the mixing of reagents with the helium buffer gas before introduction into the ion trap at (a). The new manifold allows addition of liquid reagents. The liquid reagents enter the system from a metered syringe pump (d), where they evaporate. The partial pressure of these rea-gents may be controlled through the syringe pump rate, the helium flow rate, and by heating or cooling the manifold, which is done by wrapping the manifold tubing with a temperature-controlled water coil (dashed boxes in the figure). Upon further modification, gaseous reagents will be added directly through a separate port (b). All of the gas ports are controlled by precision needle valves (N), which provide control of the flow rates. The helium buffer gas flow rate is monitored with a mass flow meter (F) and flow is controlled by the needle valve to the exhaust line (c). When operating the mass spectrometer without additional reagents, three-way valves (T) route the buffer gas through a clean section of tubing. The reagent pathway may be purged by flushing with clean gas (e.g. nitrogen) into a vacuum pump (f). The vacuum pump is preceded by a cold trap to aid in the removal of volatile reagents. The entire manifold is constructed from stainless steel tubing and components using compression fittings so that it may be periodically removed and baked in an oven for cleaning.

SUPPLEMENTARY INFORMATION

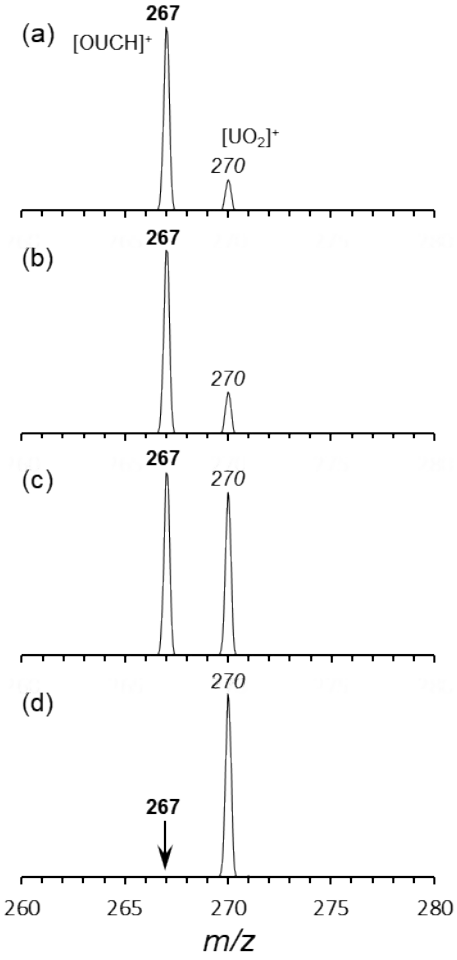

Figure S2. The product ion spectra generated by isolation (MS^6 stage) of $[OUCH]^+$ for reaction with background H_2O and O_2 in the ion trap: (a) 1 ms isolation time, (b) 10 ms isolation time, (c) 100 ms isolation time and (d) 1 s isolation time.

SUPPLEMENTARY INFORMATION

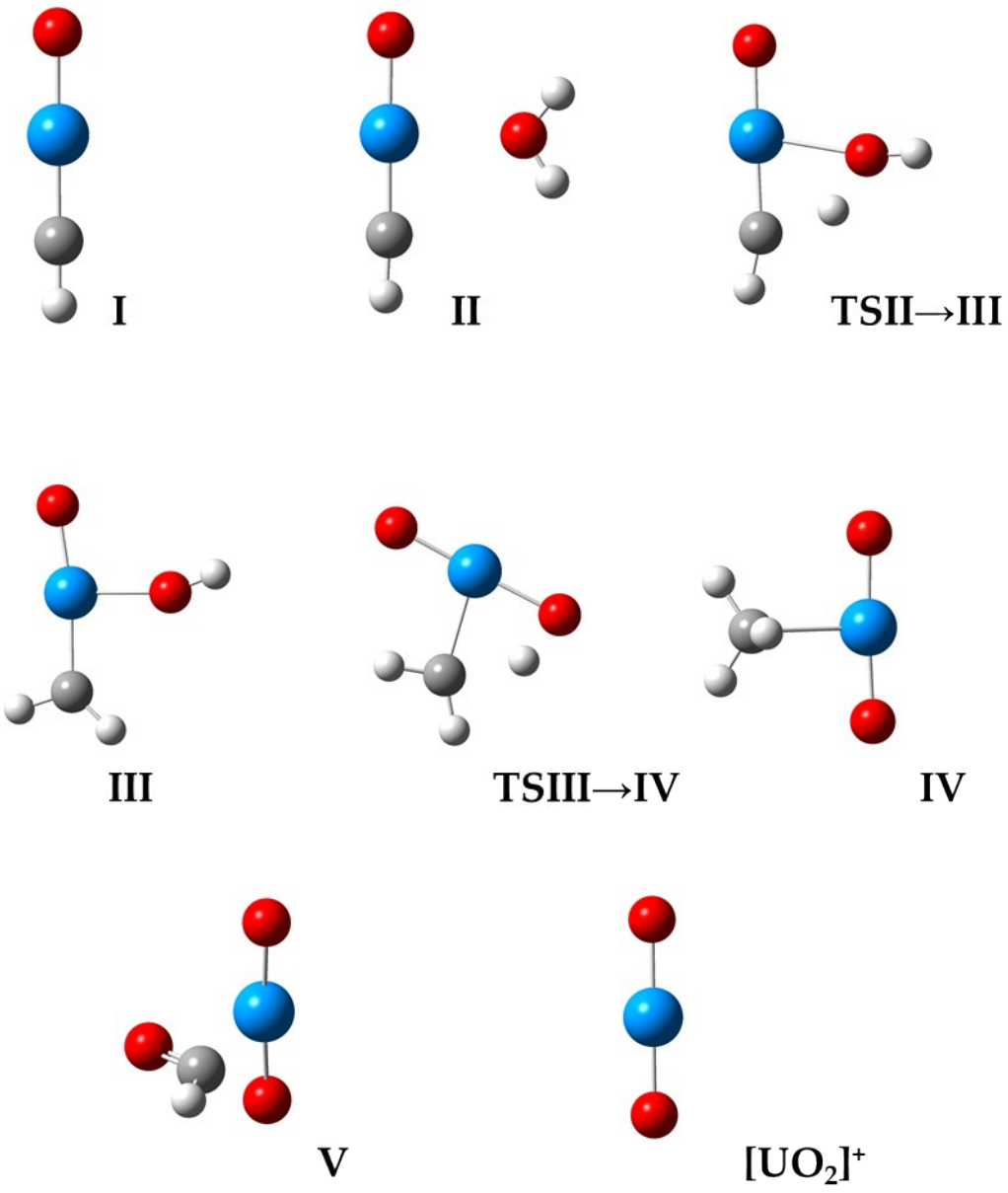

Figure S3. Structures of minima and transition states identified for reaction of $[OUCH]^+$ with H_2O and O_2. Structures were optimized at M06L/MWB60/aug-cc-pvtz level of theory.

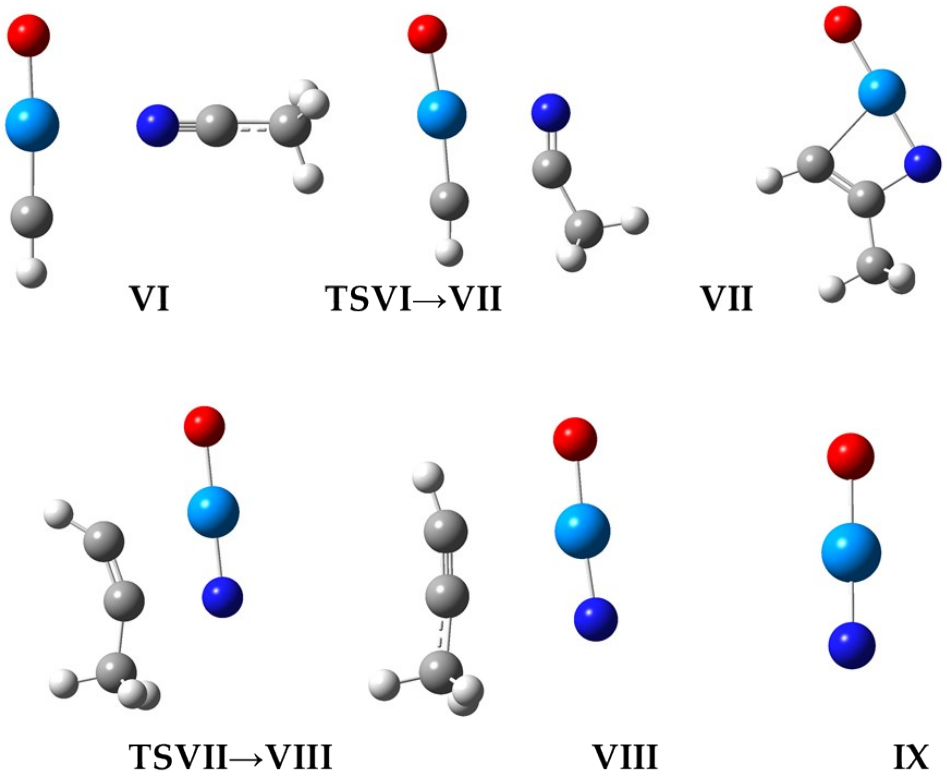

Figure S4. Structures of minima and transition states identified for reaction of $[OUCH]^+$ with $CH_3C{\equiv}N$. Structures were optimized at M06L/MWB60/aug-cc-pvtz level of theory.

SUPPLEMENTARY INFORMATION

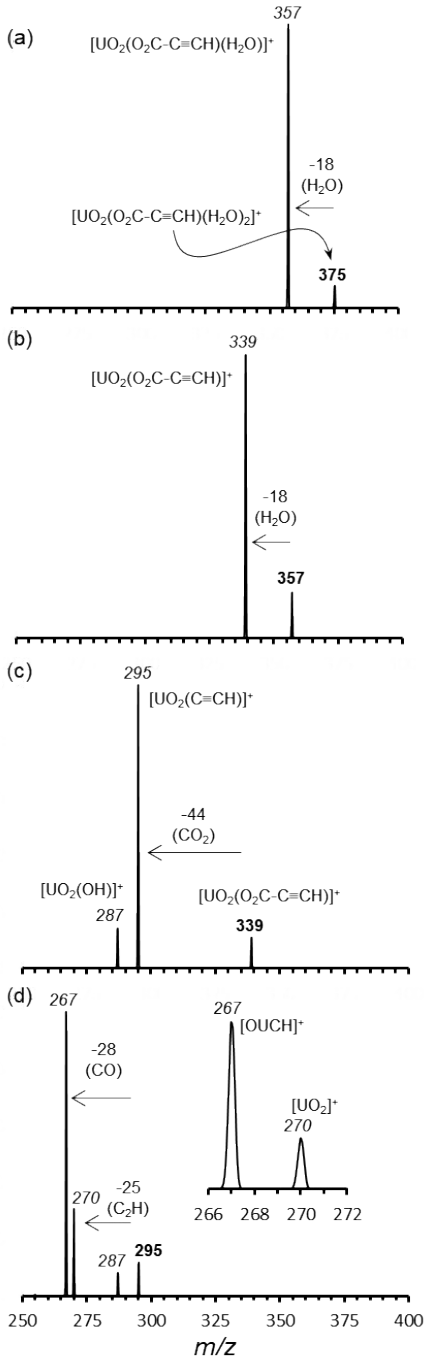

Figure S5. MS^n CID spectra derived from $[UO_2(O_2C\text{-}C{\equiv}CH)(H_2O)_2]^+$ precursor ion: (a) dissociation (MS/MS) stage of $[UO_2(O_2C\text{-}C{\equiv}CH)(H_2O)_2]^+$, (b) dissociation ($MS^3$ stage) of $[UO_2(O_2C\text{-}C{\equiv}CH)(H_2O)]^+$, (c) dissociation ($MS^4$ stage) of $[UO_2(O_2C\text{-}C{\equiv}CH)]^+$ and (d) dissociation (MS^5 stage) of $[UO_2(C{\equiv}CH)]^+$. Ions isolated for dissociation are shown in bold font, product ions are identified with italicized font.

SUPPLEMENTARY INFORMATION

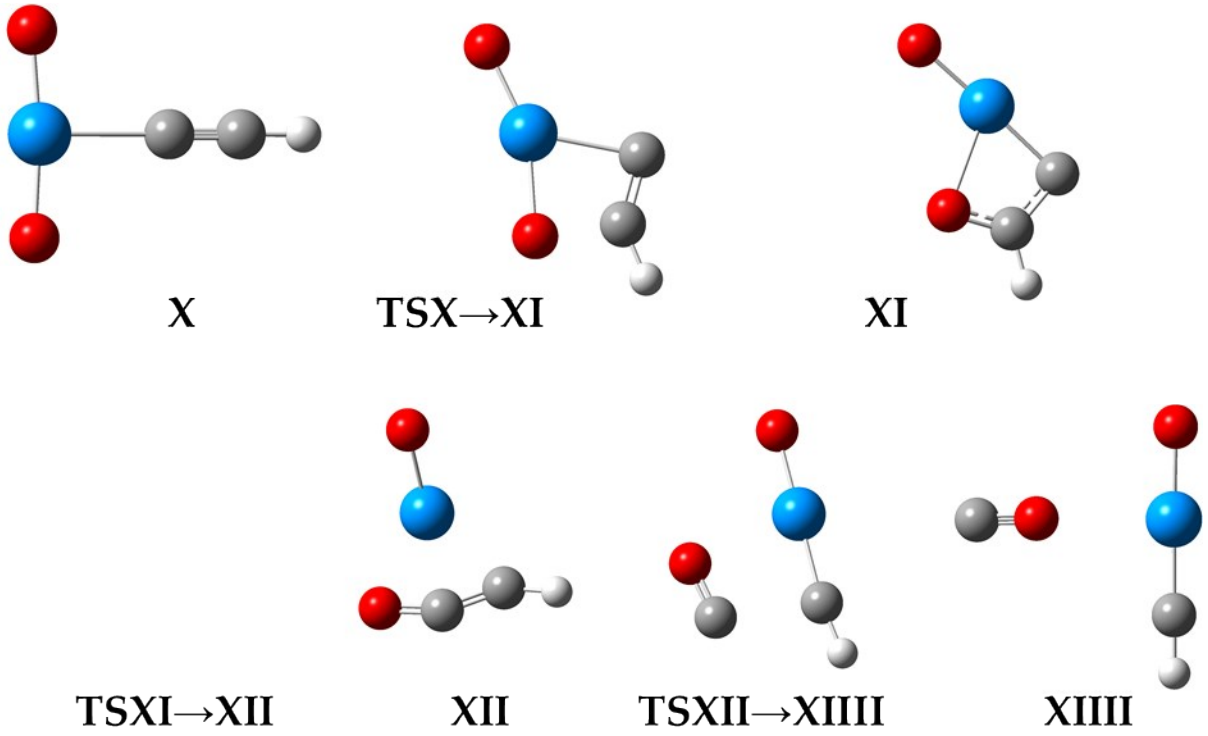

Figure S6. Structures of minima and transition states identified for creation of $[OUCH]^+$ from $[UO_2(C{\equiv}CH)]^+$ by collision-induced dissociation. Structures were optimized at M06L/MWB60/aug-cc-pvtz level of theory.

SUPPLEMENTARY INFORMATION

Table S1.

Singlet State	Structure	Electronic energy (E)	Zero-point correction (ZPE)	E+ZPE
PBE0	I	-590.4337	0.0148	-590.4188
	H_2O	-76.3800	0.0215	-76.3584
	II	-666.8727	0.0405	-666.8322
	TSII→III	-666.8453	0.0347	-666.8106
	III	-666.9037	0.0380	-666.8656
	TSIII→IV	-666.8591	0.0348	-666.8243
	IV	-666.9579	0.0393	-666.9186
	$[UO_2]^+$	-627.1212	0.0050	-627.1162
	$\bullet CH_3$	-39.7993	0.0298	-39.7696
	O_2	-150.2302	0.0062	-150.2263
	V	-740.9451	0.0239	-740.9211
	Structure	Electronic energy (E)	Zero-point correction (ZPE)	E+ZPE
M06L	I	-590.637815	0.0147	-590.6231
	H_2O	-76.444768	0.0215	-76.4233
	II	-667.140056	0.0401	-667.1000
	TSII→III	-667.111778	0.0345	-667.0773
	III	-667.173055	0.0371	-667.1360
	TSIII→IV	-667.13511	0.0339	-667.1012
	IV	-667.234088	0.0385	-667.1956
	$[UO_2]^+$	-627.349828	0.0048	-627.3450
	$\bullet CH_3$	-39.844843	0.0291	-39.8157
	O_2	-150.3585	0.0037	-150.3548
	V	-741.2868	0.0230	-741.2638
Triplet State	Structure	Electronic energy (E)	Zero-point correction (ZPE)	E+ZPE
PBE0	I	-590.412788	0.012337	-590.400451
	H_2O	-76.379984	0.021544	-76.35844
	II	-666.84735	0.037962	-666.809387
	TSII→III	-666.822365	0.034733	-666.787632
	III	-666.894024	0.036373	-666.857651
	TSIII→IV	-666.871306	0.033852	-666.837454
	IV	-666.947272	0.037371	-666.9099
	Structure	Electronic energy (E)	Zero-point correction (ZPE)	E+ZPE
M06L	I	-590.621401	0.011958	-590.609442
	H_2O	-76.444768	0.021493	-76.423276
	II	-667.120343	0.037394	-667.082949
	TSII→III	-667.091482	0.031545	-667.059937
	III	-667.163999	0.042836	-667.128321
	TSIII→IV	-667.137795	0.032389	-667.105406
	IV	-667.215571	0.037343	-667.178228

SUPPLEMENTARY INFORMATION

Table S2.

Singlet State	Structure	Electronic energy (E)	Zero-point correction (ZPE)	E+ZPE
PBE0	$CH_3C{\equiv}N$	-132.639336	0.045348	-132.593987
	VI	-723.145512	0.061763	-723.083749
	TSVI→VII	-723.133145	0.061824	-723.071322
	VII	-723.182352	0.064819	-723.117533
	TSVII→VIII	-723.166717	0.063052	-723.103665
	VIII	-723.174948	0.062828	-723.11212
	IX	-606.568594	0.005499	-606.563095
	$HC{\equiv}C\text{-}CH_3$	-116.546107	0.055745	-116.490361

Singlet State	Structure	Electronic energy (E)	Zero-point correction (ZPE)	E+ZPE
M06L	$CH_3C{\equiv}N$	-132.784444	0.045442	-132.739002
	VI	-723.494009	0.061398	-723.432611
	TSVI→VII	-723.479023	0.06168	-723.417343
	VII	-723.525242	0.063984	-723.461258
	TSVII→VIII	-723.506476	0.062441	-723.444035
	VIII	-723.518876	0.062317	-723.456559
	IX	-606.780161	0.005149	-606.775012
	$HC{\equiv}C\text{-}CH_3$	-116.679544	0.055871	-116.623673

Triplet State	Structure	Electronic energy (E)	Zero-point correction (ZPE)	E+ZPE
PBE0	VI	-723.122112	0.061763	-723.060349
	TSVI→VII	-723.108761	0.061824	-723.046937
	VII	-723.151751	0.062494	-723.089257
	TSVII→VIII	-723.115197	0.063052	-723.052145
	VIII	-723.124189	0.061673	-723.062517
	IX	-606.520678	0.004827	-606.515851

Triplet State	Structure	Electronic energy (E)	Zero-point correction (ZPE)	E+ZPE
M06L	VI	-723.473439	0.058932	-723.414507
	TSVI→VII	-723.454573	0.061824	-723.392749
	VII	-723.500711	0.06319	-723.43752
	TSVII→VIII	-723.464605	0.061434	-723.403172
	VIII	-723.481706	0.061626	-723.42008
	IX	-606.751979	0.00461	-606.74737

SUPPLEMENTARY INFORMATION

Singlet State	Structure	Electronic energy (E)	Zero-point correction (ZPE)	E+ZPE
PBE0	X	-703.762181	0.02366	-703.738521
	TSX→XI	-703.691151	0.023782	-703.667368
	XI	-703.705588	0.025637	-703.67995
	TSXI→XII	-703.618549	0.019021	-703.599528
	XII	-703.682352	0.024638	-703.687183
	TSXII→XIII	-703.674089	0.022223	-703.651865
	XIII	-703.677765	0.021304	-703.656462
	I	-590.433673	0.014835	-590.418839
	CO	-113.22703	0.005089	-113.221941
	$[UO_2]^+$	-627.1212	0.0050	-627.1162
	•C≡CH	-76.53506	0.013793	-76.521267

Singlet State	Structure	Electronic energy (E)	Zero-point correction (ZPE)	E+ZPE
M06L	X	-704.080264	0.022994	-704.05727
	TSX→XI	-704.012815	0.023291	-703.989523
	XI	-704.01762	0.02454	-703.99308
	TSXI→XII	-703.941376	0.018496	-703.92288
	XII	-704.0287	0.023953	-704.004747
	TSXII→XIII	-703.987329	0.021761	-703.965568
	XIII	-703.993043	0.020967	-703.972076
	I	-590.637815	0.0147	-590.623115
	CO	-113.337234	0.005004	-113.33223
	$[UO_2]^+$	-627.349828	0.0048	-627.3450
	•C≡CH	-76.613293	0.015801	-76.597492

Triplet State	Structure	Electronic energy (E)	Zero-point correction (ZPE)	E+ZPE
PBE0	X	-703.707816	0.02197	-703.685846
	TSX→XI	-703.69149	0.022543	-703.668947
	XI	-703.710834	0.024724	-703.68611
	TSXI→XII	-703.657854	0.019436	-703.638418
	XII	-703.758959	0.024666	-703.734292
	TSXII→XIII	-703.650395	0.019262	-703.631134
	XIII	-703.646485	0.019522	-703.626964
	I	-590.412788	0.012337	-590.400451

Triplet State	Structure	Electronic energy (E)	Zero-point correction (ZPE)	E+ZPE
M06L	X	-704.031955	0.021999	-704.009956
	TSX→XI	-704.005065	0.022149	-703.982916
	XI	-704.026355	0.024134	-704.002221
	TSXI→XII	-703.980224	0.019757	-703.960467
	XII	-704.076194	0.024318	-704.051876
	TSXII→XIII	-703.969404	0.018064	-703.95134
	XIII	-703.975698	0.018351	-703.957347
	I	-590.621401	0.011958	-590.609442

Table S3

SUPPLEMENTARY INFORMATION

DESCRIPTION OF EXPERIMENTAL METHODS

Sample Preparation

Methanol (CH_3OH), acetonitrile ($CH_3C{\equiv}N$) and isotopically labeled (^{18}O) H_2O were purchased from Sigma-Aldrich Chemical (St. Louis, MO) and used as received. A sample of uranyl propiolate was prepared by combining 2-3 mg of (natural abundance) $U^{VI}O_3$ (Strem Chemicals, Newburyport MA), corresponding to approximately 7×10^{-6} to 1×10^{-5} moles, with a 2-fold mole excess of propiolic acid (Sigma Aldrich, St. Louis MO) and 400 μL of deionized/distilled H_2O in a glass scintillation vial. The solutions were allowed to incubate on a hot plate at 70°C for 12 hours. *Caution: uranium oxide is radioactive (α- and γ-emitter), and proper shielding, waste disposal and personal protective gear should be used when handling the material*. When cooled, 20 μL of the resulting solution was diluted with 800 μL of 90:10 (by volume) H_2O: CH_3OH and used without further work up as the spray solution for ESI-MS. The methanol co-solvent was necessary to create stable spray conditions for ion formation.

Mass Spectrometry Experiments

ESI and CID experiments were performed on a ThermoScientific (San Jose, CA) LTQ-XL linear ion trap (LIT) mass spectrometer. Solutions for ESI were infused into the instrument using the incorporated syringe pump at a flow rate of 5 μL/min. The atmospheric pressure ionization stack settings of the LTQ-XL (lens voltages, quadrupole and octopole voltage offsets, etc.) were optimized for maximum transmission of singly-charged ions such as $[UO_2(O_2C\text{-}C{\equiv}CH)(H_2O)_2]^+$ to the ion trap using the auto-tune routine within the LTQ Tune program. Helium was used as the bath/buffer gas to improve trapping efficiency and as the collision gas for CID experiments.

An attractive feature of the LIT, and quadrupole ion traps in general, is that it allows "tandem in time" CID experiments, with several collisional-activation steps in series, initiated with a given precursor ion[26]. In the MS^n CID experiments in this study, precursor ions were isolated using a width of 1.0 to 1.5 mass to charge (m/z) units centered on the ^{238}U isotope. The exact value was determined empirically to provide maximum ion intensity while ensuring

isolation of a single isotopic peak. To probe CID behavior, the (mass) normalized collision energy (NCE, as defined by ThermoScientific) was set between 5 and 18%, which corresponds to 0.075 - 0.27 V applied for CID with the current instrument calibration. The activation Q, which defines the frequency of the applied radio frequency potential, was set at 0.30 and a 30 ms activation time was used.

We have installed a gas manifold on the buffer gas inlet of our instrument (**Figure S1** of the supporting information) to allow the mixing of reagents with the helium buffer gas before introduction into the ion trap. Liquid reagents are introduced into the manifold from a metered syringe pump, where they evaporate. The partial pressure of these reagents may be controlled through the syringe pump rate, the helium flow rate, and by heating or cooling the manifold, which is done by wrapping the manifold tubing with a temperature-controlled water coil. All gas ports are controlled by manually actuated precision needle valves, which provide control of the flow rates. The helium buffer gas flow rate is monitored with an electronic mass flow meter and flow is controlled by the needle valve to the exhaust line. When operating the mass spectrometer without additional reagents, three-way valves route the buffer gas through a clean section of tubing. The reagent pathway may be purged by flushing with clean gas (e.g. nitrogen) into a vacuum pump. The vacuum pump is preceded by a cold trap to aid in the removal of volatile reagents. The entire manifold is constructed from stainless steel tubing and components using stainless steel compression fittings, so that it may be periodically removed and baked in an oven for cleaning.

To probe gas-phase reactions of selected precursor ions with background neutrals, ions were isolated using widths of 1-2 *m*/*z* units. Here too, the specific width used was chosen empirically to ensure maximum ion isolation efficiency. The ions were then stored in the LIT for periods ranging from 1 ms to 10 s. When examining ion-molecule reactions (IMRs), our intent was not to measure or report rates or rate constants, but to identify the *pathways* by which ions react with neutrals such as H_2O or $CH_3C{\equiv}N$ in the LIT. Because the experiments were performed using the multi-dimensional tandem mass spectrometry capabilities of the linear ion trap, care had to be taken to ensure that enough neutral reagent was present in the ion trap for ion-molecule reaction studies, without hampering the "synthesis" of the [OUCH]+ precursor

ion by repeated CID steps. For both CID and IMR experiments, the mass spectra displayed were created by accumulating and averaging at least 30 isolation, dissociation, and ejection/detection steps.

Computational Methodology

While the objective was to generate data regarding the gas-phase reactions of $[OUCH]^+$ with H_2O, O_2 and $CH_3C{\equiv}N$, supporting DFT calculations can provide important insight into reaction mechanisms and relative energetics. For the reactions that were the focus of this study, the structures of the various isomers, reaction intermediates, and transition states, were optimized using two different density functionals (PBE0 and M06-L), which were chosen based on the good performance when investigating reaction pathways and energetics for uranyl species in our prior studies[1-3]. The MWB60 pseudopotential and associated basis set was used on U and the aug-cc-pvtz basis set on all other atoms. Transition states were identified using the QST2 and QST3 approaches[4-7] and were confirmed by means of intrinsic reaction coordinate calculations. The Gaussian 16 software package[8] was used for all calculations.

Singlet-state optimizations were performed within the restricted Kohn−Sham formalism, whereas triplet-state species were studied using the unrestricted approach. We note here that our intent was not to rigorously assess the accuracy of DFT for determining reaction thermochemistry, bond lengths and angles, or bond-dissociation energies, but instead to identify probable reaction pathways "in-silico" that reproduce the experimental observations in terms of dissociation or ion-molecule reactions. DFT has been used in several previous studies to probe the properties of gas-phase uranyl species[9-20]. In the present study, we found good agreement between the relative energies obtained at PBE0 and M06-L levels - the two theory levels predict the same pathways and the same ordering of energy states. Because we have had greater success with the Minnesota functional when elucidating reaction pathways, the computational results generated at the M06-L level of theory are discussed for the sake of brevity.

It should be noted that spin−orbit corrections were not explicitly included in our calculations. Although spin−orbit effects are not expected to significantly affect the energetics

of processes in which there is no change in the formal oxidation state of the heavy metal, substantial changes can occur for reaction energies involving actinide atoms in different oxidation states. While it is possible that the energies of specific species with U in different oxidation states could be affected by the inclusion of spin−orbit corrections, we feel that this caveat does not influence our interpretation of the DFT investigation of likely reaction mechanisms.

1. M. J. Van Stipdonk, M. del Carmen Michelini, A. Plaviak, D. Martin, J. K. Gibson, Formation of bare UO_2^{2+} and NUO^+ by fragmentation of gas-phase uranyl-acetonitrile complexes. *J. Phys. Chem. A*. 2014, **118**, 7838 – 7846.

2. C. M. Leavitt, V. S. Bryantsev, W. A. de Jong, M. S. Diallo, W. A. Goddard III, G. S. Groenewold, M. J. Van Stipdonk, Addition of H_2O and O_2 to acetone and dimethylsulfoxide ligated uranyl(V) dioxocations. *J. Phys. Chem. A*. 2009, **113**, 2350 – 2358.

3. M. Van Stipdonk, E. Perez, C. Hanley, I. Tatosian, A. Bubas, S. Kline, Formation and hydrolysis of gas-phase $[U^{VI}O_{2(}R)]^+$ [R=CH_3, CH_2CH_3, $CH{=}CH_2$ and C_6H_5]. *J. Mass Spectrom. 2019,* **54**, 780 – 789.

4. C. Peng, H. B. Schlegel. Combining synchronous transit and quasi-Newton methods for finding transition states. *Israel J. Chem*. **1993**, *33*, 449 – 454.

5. K. Fukui, The Path of Chemical-Reactions - The IRC Approach. *Acc. Chem. Res*. 1981, **14**, 363−368.

6. C. Gonzalez, H. B. Schlegel, An Improved Algorithm for Reaction-Path Following. *J. Chem. Phys*. 1989, **90**, 2154 – 2161.

7. C. Gonzalez, H. B. Schlegel, Reaction-Path Following in Mass-Weighted Internal coordinates. *J. Phys. Chem*. 1990, **94**, 5523 – 5527.

8. Gaussian 09, Revision A.02, M. J. Frisch, G. W. Trucks, H. B. Schlegel, G. E. Scuseria, M. A. Robb, J. R. Cheeseman, G. Scalmani, V. Barone, G. A. Petersson, H. Nakatsuji, X. Li, M. Caricato, A. Marenich, J. Bloino, B. G. Janesko, R. Gomperts, B. Mennucci, H. P. Hratchian, J. V. Ortiz, A. F. Izmaylov, J. L. Sonnenberg, D. Williams-Young, F. Ding, F. Lipparini, F. Egidi, J. Goings, B. Peng, A. Petrone, T. Henderson, D. Ranasinghe, V. G. Zakrzewski, J. Gao, N. Rega, G. Zheng, W. Liang, M. Hada, M. Ehara, K. Toyota, R. Fukuda, J. Hasegawa, M. Ishida, T. Nakajima, Y. Honda, O. Kitao, H. Nakai, T. Vreven, K. Throssell, J. A. Montgomery, Jr., J. E. Peralta, F. Ogliaro, M. Bearpark, J. J. Heyd, E. Brothers, K. N. Kudin, V. N. Staroverov, T. Keith, R. Kobayashi, J. Normand, K. Raghavachari, A. Rendell, J. C. Burant, S. S. Iyengar, J. Tomasi, M.

SUPPLEMENTARY INFORMATION

Cossi, J. M. Millam, M. Klene, C. Adamo, R. Cammi, J. W. Ochterski, R. L. Martin, K. Morokuma, O. Farkas, J. B. Foresman, and D. J. Fox, Gaussian, Inc., Wallingford CT, 2016.

9. M. J. van Stipdonk, I. J. Tatosian, A. C. Iacovino, A. R. Bubas, L. Metzler, M. C. Sherman, A. Somogyi, Gas-phase deconstruction of UO_2^{2+}: Mass spectrometry evidence for generation of $[OU^{VI}CH]^+$ by collision-induced dissociation of $[U^{VI}O_2(C{\equiv}CH)]^+$. *J. Am. Soc. Mass Spectrom.* 2019, **30**, 796 – 805.

10. Y. Gong, V. Vallet, M. Michelini, D. Rios, J. K. Gibson, Activation of gas-phase uranyl: from and oxo to a nitrido complex. *J. Phys. Chem. A*. 2014, **118**, 325 – 330.

11. Y. Gong, W. A.; de Jong, J. K. Gibson, Gas phase uranyl activation: formation of a uranium nitrosyl complex from uranyl azide. *J. Am. Chem. Soc*. 2015, **137**, 5911 – 5915.

12. S.-X. Hu, J. Jian, J. Li, J. K. Gibson, Destruction of the uranyl moiety in a U(V) "cation-cation" interaction. *Inorg. Chem*. 2019, **58**, 10148 – 10159.

13. V. Vallet, U. Wahlgen, I. Grenthe, Probing the nature of chemical bonding in uranyl(VI) complexes with quantum chemical methods, *J. Phys. Chem. A* 2012, **116**, 12373 – 12380.

14. J. Su, P. D. Dau, Y.-H. Qui, H.-T. Liu, C.-F. Xu, D.-L. Huang, L.-S. Wang, J. Li, Probing the electronic structure and chemical bonding in tricoordinate uranyl complexes $UO_2X_3^-$ (X=F, Cl, Br, I): competition between coulomb repulsion and U-X bonding, *Inorg. Chem*. 2013, **52**, 6617 – 6626.

15. W. A. De Jong, E. Apra, T. L. Windus, J. A. Nichols, R. J. Harrison, K. E. Gutowski, D. A. Dixon, Complexation of the Carbonate, Nitrate, and Acetate Anions with the Uranyl Dication: Density Functional Studies with Relativistic Effective Core Potentials. *J. Phys. Chem. A* 2005, **109**, 11568 – 11577.

16. V.E. Jackson, R. Craciun, D.A. Dixon, K.A. Peterson, W.A. de Jong, Prediction of Vibrational Frequencies of UO_2^{2+} at the CCSD(T) Level, *J. Phys. Chem. A* 2008, **112** 4095 – 4099.

17. M. García-Hernández, C. Willnauer, S. Krüger, L. V. Moskaleva, N. Rösch. Systematic DFT Study of Gas Phase and Solvated Uranyl and Neptunyl Complexes $[AnO_2X_4]^n$ (An = U, Np; X = F, Cl, OH, n = −2; X = H_2O, n = +2) *Inorg. Chem.* 2006, **45**, 3, 1356 – 1366

18. D. Rios, M. C. Michelini, A. F. Lucena, J. Marçalo, T. H. Bray, J. K. Gibson. Gas-Phase Uranyl, Neptunyl, and Plutonyl: Hydration and Oxidation Studied by Experiment and Theory *Inorg. Chem.* 2012, **51**, 6603 – 6614.

19. P. D. Dau, P. B. Armentrout, M. C. Michelini, J. K. Gibson, Activation of carbon dioxide by a terminal uranium–nitrogen bond in the gas-phase: a demonstration of the principle of microscopic reversibility, *Phys. Chem. Chem. Phys*., 2016, **18**, 7334 – 7340

SUPPLEMENTARY INFORMATION

20. Di Santo, Emanuela; Michelini, Maria del Carmen; Russo, Nino, Methane C-H Bond Activation by Gas-Phase Th^+ and U^+: Reaction Mechanisms and Bonding Analysis. *Organometallics*, 2009, 28, 3716-3726

48. Michelini, Maria del Carmen; Russo, Nino; Sicilia, Emilia, How can uranium ions (U^+, U^{2+}) activate the O-H bond of water in the gas phase? *Angew. Chemie, Int. Ed.*, 2006, 45, 1095-1099.

49. Garrison, Stephen L.; Becnel, James M. Transition State for the Gas-Phase Reaction of Uranium Hexafluoride with Water. *J. Phys. Chem. A*, 2008, 112, 5453-5457.

50. Alikhani, Mohammad Esmail; Michelini, Maria del Carmen; Russo, Nino; Silvi, Bernard. Topological Analysis of the Reaction of Uranium Ions (U^+, U^{2+}) with N_2O in the Gas Phase. *J. Phys. Chem. A*, 2008, 112, 12966-12974.

51. Di Santo, Emanuela; Santos, Marta; Michelini, Maria C.; Marcalo, Joaquim; Russo, Nino; Gibson, John K. Gas-Phase Reactions of the Bare Th^{2+} and U^{2+} Ions with Small Alkanes, CH_4, C_2H_6, and C_3H_8: Experimental and Theoretical Study of Elementary Organoactinide Chemistry. *J. Am. Chem. Soc*. 2011, 133, 1955-1970.

52. Shi, Ling; Li, Peng; Guo, Ming-gang; Gao, Tao. Reaction mechanisms and topological analyses for the C-H activation of ethylene by uranium atom using density functional theory. *Comput Theor Chem*, 2020, 1190, 113022.

53. Daniel Rios, Maria del Carmen Michelini, Ana F. Lucena, Joaquim Marçalo, and John K. Gibson, On the Origins of Faster Oxo Exchange for Uranyl(V) versus Plutonyl(V), *J. Am. Chem. Soc*. 2012, **134**, 15488–15496.